

## A Study on the Electrochemical Behavior of a L245NB/316L Bimetallic Composite in CO<sub>2</sub>-Saturated Solutions with Different S<sup>2-</sup> Concentrations

Jiaji Zhang<sup>1</sup>, Shuliang Wang<sup>1,\*</sup>, Hao Tan<sup>1</sup>, Feng Wang<sup>1</sup>, Li Liu<sup>1</sup>, Chunyan Fu<sup>1,\*</sup>, Dinghan Xiang<sup>2</sup>

<sup>1</sup> School of New Energy and Materials, Southwest Petroleum University, Xindu Avenue 8#, Sichuan 610500, China

<sup>2</sup> Guangxi Key Laboratory of Information Materials, Guilin University of Electronic Technology, Guilin 541004, PR China;

\*E-mail: [wsliang1465@126.com](mailto:wsliang1465@126.com) (S.L. Wang), [253105267@qq.com](mailto:253105267@qq.com) (C.Y. Fu)

Received: 27 August 2020 / Accepted: 5 October 2020 / Published: 31 October 2020

---

An investigation on the electrochemical behavior of the base and weld metals of the inner wall of an L245NB/316L bimetallic composite pipe in carbon dioxide (CO<sub>2</sub>-saturated and CO<sub>2</sub>-free environments with different S<sup>2-</sup> concentrations) was conducted using potentiodynamic polarization and electrochemical impedance spectroscopy (EIS) techniques. Results demonstrated that the electrochemical reaction rate showed an increasing trend with increasing S<sup>2-</sup> concentration, and CO<sub>2</sub> and S<sup>2-</sup> synergistically accelerated the electrochemical reaction rate when the concentration of S<sup>2-</sup> was lower than 0.1 mol/l. For the weld metal, however, the electrochemical reaction rate decreased due to the synergistic inhibition effect of CO<sub>2</sub> and S<sup>2-</sup> when the concentration of S<sup>2-</sup> was increased to 0.5 mol/l. The corrosion resistance of the weld metal was significantly lower than that of the base metal under the same testing conditions.

---

**Keywords:** L245NB/316L bimetallic composite pipe; Weld joint; Electrochemistry; S<sup>2-</sup> concentration; Carbon dioxide

### 1. INTRODUCTION

Carbon steel is commonly used as a construction material in oil and gas fields due to its excellent mechanical properties and low cost. However, its poor corrosion resistance significantly limits its structural safety and reliability. Stainless steels or corrosion-resistant alloys can be used as an option when long-term corrosion resistance is required, but their cost is comparatively high. Thus, bimetallic composite pipes that have an outer strengthening layer of carbon steel and an inner corrosion-resistant layer of stainless steel are widely used as a compromise for the manufacture of gathering and transportation pipelines[1]. For example, a corrosion-resistant 316L stainless steel layer is usually

welded to an outer carbon steel layer to reduce the corrosion of pipeline steels in harsh environments with high H<sub>2</sub>S and CO<sub>2</sub> contents during oil and gas exploitation, transportation and refining processes[2-5]. Therefore, the corrosion behavior of the welded portion of a bimetallic composite pipe must be investigated to ensure safety during operations in oil and gas fields.

During the production and transportation of oil and gas in the field, there are some corrosive media, including acidic CO<sub>2</sub> and H<sub>2</sub>S gases, Cl<sup>-</sup>, etc., which make pipelines extremely vulnerable to corrosion damage[6-9]. Although dry CO<sub>2</sub> and H<sub>2</sub>S gases are not corrosive to steel, the formation of acidic solutions with the dissolution of these gases in water will promote severe corrosion of the pipeline steel[10-12]. In regard to H<sub>2</sub>S corrosion, the anodic reaction[13-14] is a dissolution of iron and the formation of iron-rich FeS<sub>1-x</sub> and sulfur-rich FeS<sub>1+x</sub>, whereas the cathodic reaction is a competitive reaction relevant to depolarizers such as H<sub>2</sub>S, HS<sup>-</sup> and H<sup>+</sup>. The dissociation products of H<sub>2</sub>S, i.e., HS<sup>-</sup> and S<sup>2-</sup> are prone to adsorb on steel surfaces, leading to the formation of an adsorption complex ion (Fe(HS)<sup>-</sup>). The existence of HS<sup>-</sup> and S<sup>2-</sup> will negatively shift the corrosion potential and increase the rate of the hydrogen evolution reaction (HER). As a powerful depolarizer, H<sup>+</sup> is likely to obtain electrons on the cathode. Additionally, H<sup>+</sup> can significantly weaken the strength of the metallic bond between iron atoms, thus accelerating the rate of anodic dissolution. Previous studies revealed that the presence of S<sup>2-</sup> was the main cause of iron corrosion in the above-discussed process, in which the concentration of S<sup>2-</sup> played a critical role[15]. S<sup>2-</sup> and its incomplete oxidation compounds can oxidize on the anode and cause corrosion; then, the oxidation products on the anode migrate to the cathode and affect the cathode reaction[16]. Since H<sub>2</sub>S is always accompanied by CO<sub>2</sub> during oil and gas field exploitation, it is necessary to realistically study the corrosion of pipeline steels in a H<sub>2</sub>S/CO<sub>2</sub>-containing environment. However, many past studies have focused on the corrosion behavior of a single metal in H<sub>2</sub>S/CO<sub>2</sub> environments[17-18], and studies on the corrosion behavior of the base and weld metals of bimetallic composite pipes by S<sup>2-</sup> and CO<sub>2</sub> are relatively few.

This work aims to examine the electrochemical behavior of a base metal (316L) and weld metal of the inner wall of an L245NB/316L bimetallic composite pipe in a carbon dioxide-saturated environment and carbon dioxide-free environment with various S<sup>2-</sup> concentrations. Results illustrate the mechanism of electrochemical corrosion caused by the S<sup>2-</sup> concentration and CO<sub>2</sub>. Thus, the findings of this work could be used to predict the potential danger caused by corrosion and reduce possible economic losses during pipeline operation.

## 2. EXPERIMENTAL

### 2.1 Sample preparation and testing conditions

In this work, the experimental material was an industrial grade L245NB/316L bimetal composite seamless steel pipe with a diameter of 168.3 mm. It was TIG welded, and the welding wire material was eni6625. The samples used in the electrochemical analysis were cut from the weld joint (weld metal) and the portion far away from the weld joint (base metal) on the inner wall of the L245NB/316L bimetallic composite pipe. The dimensions of the samples for electrochemical measurement were 10

mm×10 mm×3 mm. The dimensions of the samples for the galvanic corrosion measurements were 50 mm×50 mm×3 mm. The chemical composition (in wt%) of the base metal (316L) was as follows: C 0.0212, Si 0.463, Mn 1.175, S 0.002, P 0.0224, Cr 16.919, Ni 10.14, Mo 2.086, N 0.0405 and an Fe balance. The surfaces of the test specimens were polished with SiC paper (from 400-1200 grit), and then polished to a mirror finish with diamond polishing paste. Next, the specimens were degreased with acetone, cleaned with distilled water and ethanol, and dried by cool air.

It was difficult to control the concentration of  $S^{2-}$  by directly introducing  $H_2S$  gas into the aqueous solution; furthermore,  $H_2S$  is a toxic gas. Therefore, in this work,  $Na_2S \cdot 9H_2O$  was dissolved in deionized water to obtain different concentrations of  $S^{2-}$  through ionization.

To produce the electrochemical solution, a 3.5% NaCl solution was deaerated with  $N_2$ , and then  $Na_2S \cdot 9H_2O$  was added. The selected concentrations of  $S^{2-}$  were 0, 0.05, 0.1 and 0.5 mol/l for studying the corrosion behavior of the base and weld metals. The solution was controlled at 60 °C by using a water bath. To study the synergistic effect of  $S^{2-}$  and  $CO_2$  on the corrosion behavior, the  $Na_2S$  solution was purged with  $CO_2$  gas for at least 4 h before the test along with purging continuously during the test to achieve a solution saturated with  $CO_2$ .

## 2.2 Galvanic corrosion test

Galvanic corrosion measurements were performed using a Zra-2 galvanic corrosion measuring instrument (ZRA) with a classical three-electrode system. The base and weld metals were connected as working electrode 1 (WE1) and working electrode 2 (WE2) to the ZRA. A saturated calomel electrode (SCE) was used as the reference electrode. An assembly diagram of the base metal (316L)/inner weld galvanic couple is shown in Figure 1. The base metal:weld metal area ratio was 1:1, and the electrode distance was 2 cm. The galvanic corrosion test was conducted in a 3.5% NaCl solution at  $60 \pm 1$  °C, and the experimental period was 120 h. The self-corrosion potentials ( $E_{k1}$ ) and ( $E_{k2}$ ), galvanic potential ( $E_g$ ) and galvanic current ( $I_g$ ) of the base and weld metal sample were recorded.

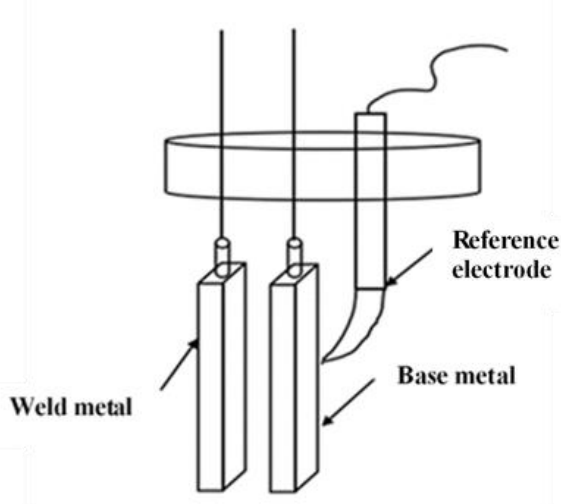


**Figure 1.** Assembly diagram of the base metal (316L)/inner weld metal galvanic couple

### 2.3 Electrochemical test

Electrochemical measurements were performed using a PGSTAT302N electrochemical workstation with a classical three-electrode system. The weld or base metal sample was used as the working electrode. A saturated calomel electrode (SCE) was used as the reference electrode, and a platinum plate was used as the auxiliary electrode.

A  $\text{Na}_2\text{S}$  solution with/without  $\text{CO}_2$  was used. Potentiodynamic polarization was performed at a scan rate of 1 mV/s from -250 (vs. open-circuit potential (OCP))-600 mV (vs. OCP). Electrochemical impedance spectroscopy (EIS) measurements were conducted at the OCP, and the EIS scanning frequency ranged from 100 kHz to 10 mHz with an AC amplitude of 10 mV (peak-to-zero). Each test was started after a 30-min stabilization period to allow the solution to achieve a relatively stable condition.

## 3. RESULTS AND DISCUSSION

### 3.1 Galvanic corrosion

#### 3.1.1 Galvanic potential of the base metal/weld metal galvanic couple

The self-corrosion potentials of the two samples at the beginning of corrosion were tested. The weld and base metal self-corrosion potentials were -400 and -388 mV, respectively. Based on the difference in potential, the potential of the weld metal was relatively negative. Therefore, the weld metal was the anode, and the base metal was the cathode[19]. Figure 2 shows the galvanic potential curves of the base metal/weld metal galvanic couple. The maximum fluctuation in the galvanic couple potential in the whole corrosion process was only 10 mV, indicating that the driving force of the galvanic couple corrosion was relatively small. The change in the galvanic potential tended to be very slight, and the galvanic corrosion was basically stable after 72 h.

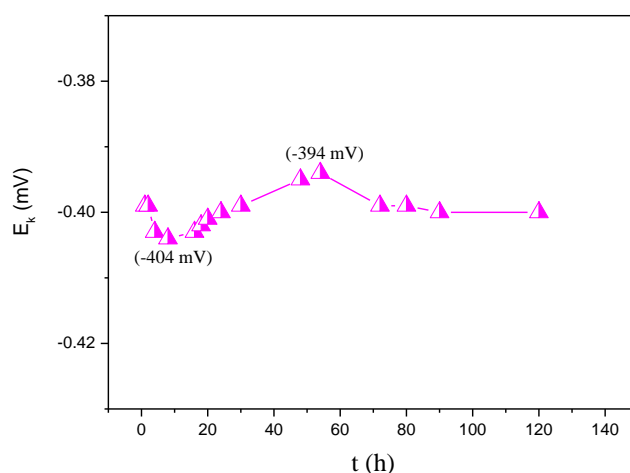


**Figure 2.** Galvanic potential curves of the base metal (316L)/weld metal galvanic couple

### 3.1.2 Galvanic current of the base metal/weld metal galvanic couple

Figure 3 shows the galvanic current curves of the galvanic couple. The rate of decrease of the galvanic current slows down within 24 h because of the formation of a protective corrosion product film. In general, the galvanic corrosion sensitivity of the galvanic couple in the electrolyte was mainly determined by the galvanic current density. In accordance with the calculation method of the galvanic current density (formula 1)[20], the galvanic current density was  $0.00218 \mu\text{A}/\text{cm}^2$ . On the basis of HB 5374, the galvanic corrosion grade of the weld and base metals was A, which indicated that the galvanic corrosion of the base and weld materials was very weak. Therefore, the galvanic corrosion of the base and weld metals could be neglected.

$$i_g = \frac{I_g}{S_a} = \frac{1}{S_a \times T} \int_0^T I_g(t) dt \quad (1)$$

where  $i_g$  is the galvanic current density,  $I_g$  is the average galvanic current,  $S_a$  is the actual area of the anode and  $T$  is the corrosion time.

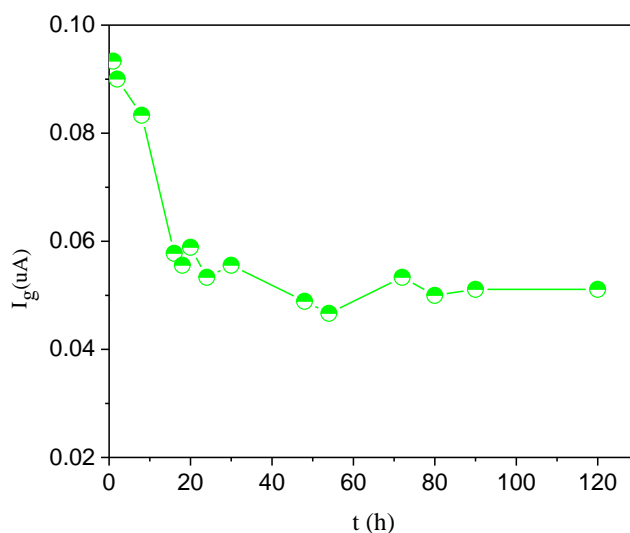


**Figure 3.** Galvanic current curves of the base metal (316L)/weld metal galvanic couple

## 3.2 Electrochemistry

### 3.2.1 Influence of the $S^{2-}$ concentration on the corrosion behavior in the absence of $CO_2$

Figure 4 shows the potentiodynamic polarization curves of the base and weld metals with various  $S^{2-}$  concentrations. The passive zone (-0.2-0.2 V) of the base metal could be seen in the absence of  $S^{2-}$ . The slope of the polarization curve decreased when  $S^{2-}$  was added to the solution, verifying that the corrosion rate increased[21]. In regard to the weld metal, when  $S^{2-}$  was added to the solution, the anodic polarization curve shifted to the left, and the tangent slope increased. The above results indicated that the anodic current density and the corrosion rate decreased because an FeS film formed on the electrode

surface[22-23], which could inhibit the anodic reaction. The polarization curve of the anode gradually shifted to the right, and the tangent slope decreased when the content of  $S^{2-}$  increased. These results indicated that the current density and corrosion rate of the anode gradually increased because the FeS film was damaged.

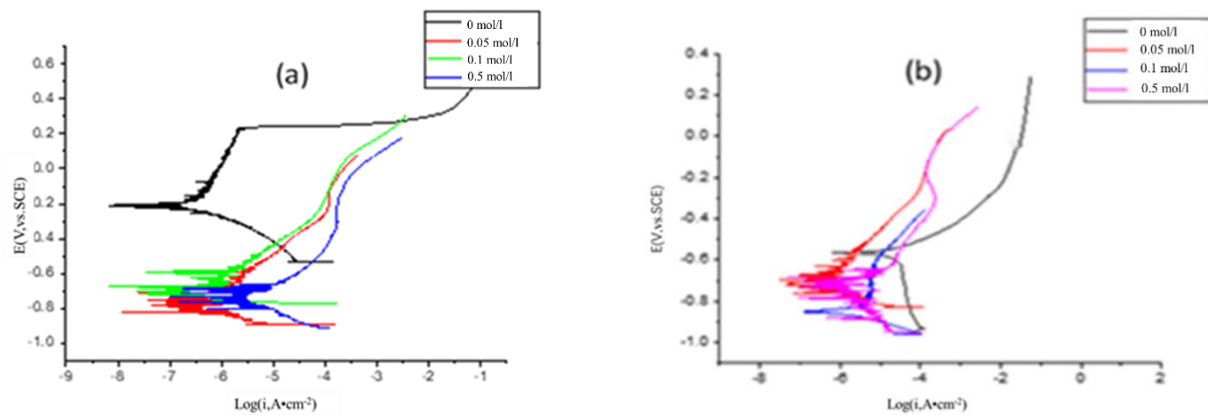


**Figure 4.** Potentiodynamic polarization curves of the base (a) and weld metals (b) with various  $S^{2-}$  concentrations at 60 °C

**Table 1.** Fitting parameters of the potentiodynamic polarization curves for samples with different  $S^{2-}$  concentrations at 60 °C.

$S^{2-}$ concentration (mol/l)	Material	$E_{corr}$ ( $V_{SCE}$ )	$i_{corr}$ ( $\mu A \cdot cm^{-2}$ )	$\beta_a$ ( $mV \cdot decade^{-1}$ )	$\beta_c$ ( $mV \cdot decade^{-1}$ )
0	Base metal	-0.199	0.349	503	141
	Weld metal	-0.526	32.35	121	126
0.05	Base metal	-0.782	0.446	220	54
	Weld metal	-0.719	0.794	230	40
0.1	Base metal	-0.662	0.955	200	70
	Weld metal	-0.843	3.467	685	50
0.5	Base metal	-0.725	5.012	200	130
	Weld metal	-0.746	7.762	267	230

The polarization curves were fitted using the Tafel extrapolation method, and the fitted parameters are listed in Table 1. In general,  $E_{corr}$  is used to describe corrosion trends, and  $I_{corr}$  can reflect corrosion rates [24-25]. The corrosion potential ( $E_{corr}$ ) of the base metal was -0.199  $V_{SCE}$  in the absence of  $S^{2-}$ . The  $E_{corr}$  decreased sharply to negative values when  $S^{2-}$  was added to the solution, implying that the presence of  $S^{2-}$  increased the trend of corrosion. With increasing concentrations of  $S^{2-}$ , the corrosion current density ( $i_{corr}$ ) had an increasing trend, as shown in Table 1. In particular, the corrosion current density increased dramatically from 0.955 to 5.012  $\mu A \cdot cm^{-2}$  when the concentration of  $S^{2-}$  was increased from 0.1 to 0.5 mol/l. For the weld metal, the  $E_{corr}$  value was -0.526  $V_{SCE}$  in the absence of  $S^{2-}$ , which was more negative than that of the base metal. The  $i_{corr}$  value of the weld metal was higher than that of

the base metal, indicating a significant decrease in the corrosion resistance after the welding process. The  $i_{\text{corr}}$  value of the weld metal decreased to  $0.794 \mu\text{A}\cdot\text{cm}^{-2}$  when a low concentration of  $\text{S}^{2-}$  (0.05 mol/l) was present. When the concentration of  $\text{S}^{2-}$  was increased, the  $i_{\text{corr}}$  value accordingly showed an increasing trend. The above results indicated that the corrosion of the weld metal was inhibited with the existence of a low concentration of  $\text{S}^{2-}$ , whereas the inhibition effect would be reduced as the concentration of  $\text{S}^{2-}$  increased. Compared to the base metal, the  $i_{\text{corr}}$  value of the weld metal was always higher at any given concentration of  $\text{S}^{2-}$ , indicating that the weld metal was prone to corrosive attack in the current investigation. The reason was probably due to the alloy elements influencing the solidification behavior of the weld metal, resulting in a low corrosion resistance of the weld metal compared with that of the base metal[26].

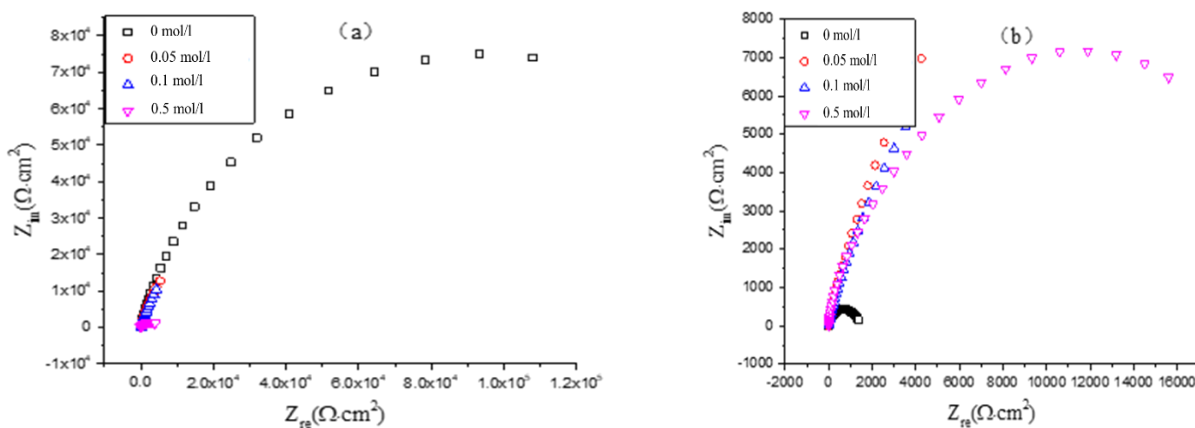


Figure 5. Nyquist plots of the base (a) and weld metals (b) with different  $\text{S}^{2-}$  concentrations at  $60\text{ }^\circ\text{C}$

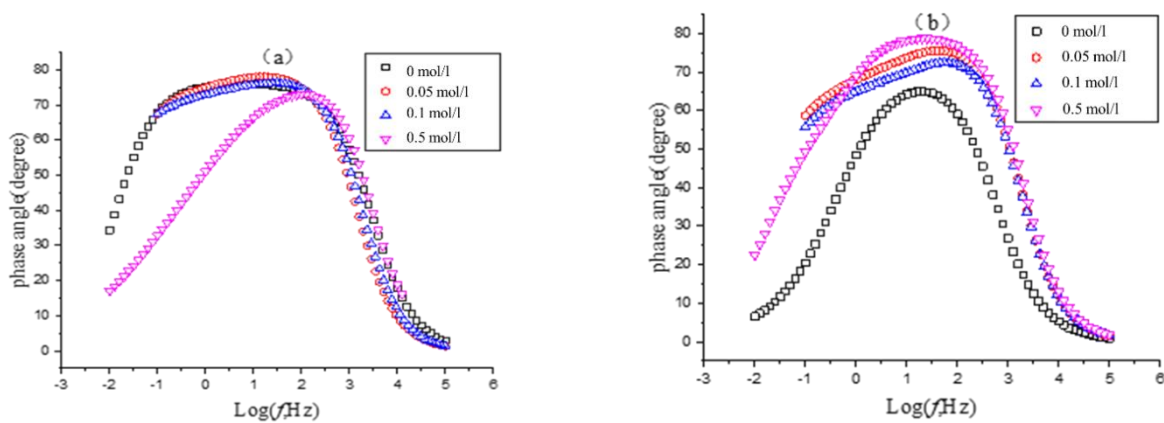
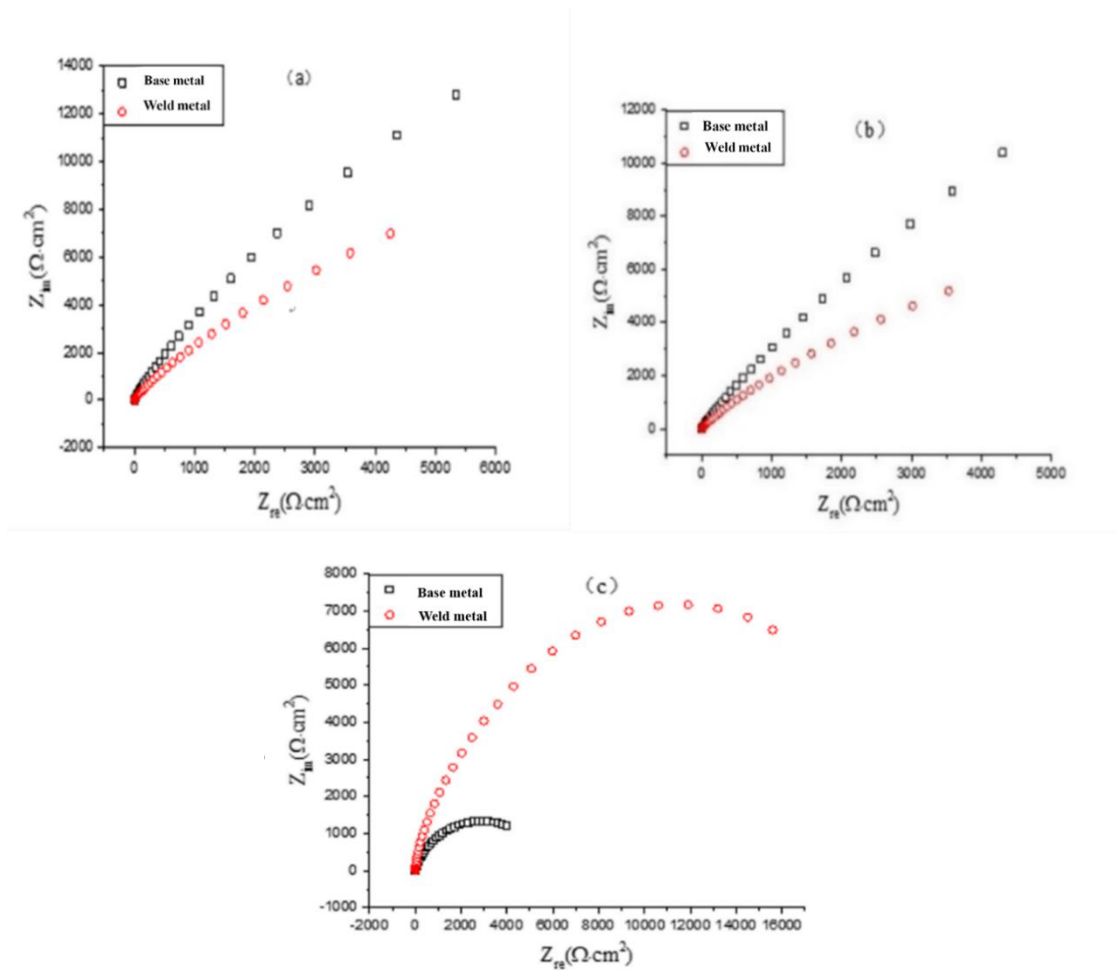
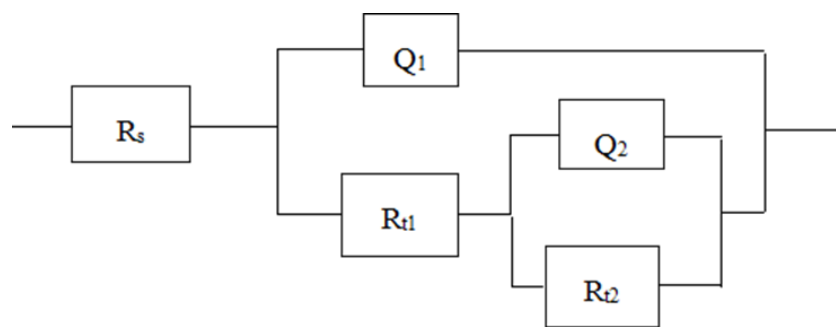


Figure 6. Bode plots of the base (a) and weld metals (b) with different  $\text{S}^{2-}$  concentrations and at  $60\text{ }^\circ\text{C}$



**Figure 7.** Comparison of the Nyquist plots for the base and weld metals with different  $\text{S}^{2-}$  concentrations at  $60 \text{ }^\circ\text{C}$ : (a)  $0.05 \text{ mol/l}$ , (b)  $0.1 \text{ mol/l}$ , and (c)  $0.5 \text{ mol/l}$



**Figure 8.** Equivalent circuit model for samples tested in the  $\text{S}^{2-}$ -containing solution

**Table 2.** EIS parameters of the base metal with different concentrations of  $\text{S}^{2-}$  at  $60 \text{ }^\circ\text{C}$

$\text{S}^{2-}$ concentration (mol/l)	$R_s$ ( $\Omega \cdot \text{cm}^2$ )	$Q_1$ ( $\Omega^{-1} \cdot \text{cm}^{-2} \cdot \text{s}^{-n}$ )	$n_1$	$R_{t1}$ ( $\Omega \cdot \text{cm}^2$ )	$Q_2$ ( $\Omega^{-1} \cdot \text{cm}^{-2} \cdot \text{s}^{-n}$ )	$n_2$	$R_2$ ( $\Omega \cdot \text{cm}^2$ )
0	4.894	$4.672 \times 10^{-5}$	0.852	$1.894 \times 10^5$	$1.291 \times 10^{-5}$	0.9227	$1.075 \times 10^5$

0.05	3.464	$8.397 \times 10^{-5}$	0.8934	6893	$2.444 \times 10^{-5}$	0.628	$1.048 \times 10^5$
0.1	2.783	$2.53 \times 10^{-5}$	1	3609	$1.019 \times 10^{-4}$	0.7499	$1.523 \times 10^5$
0.5	0.366	$3.314 \times 10^{-4}$	0.8479	1390	$9.871 \times 10^{-5}$	0.9054	$6.439 \times 10^4$

**Table 3.** EIS parameters of the weld metal with different concentrations of  $S^{2-}$  at 60 °C

$S^{2-}$ concentration (mol/l)	$R_s$ ( $\Omega \cdot \text{cm}^2$ )	$Q_1$ ( $\Omega^{-1} \cdot \text{cm}^{-2} \cdot \text{s}^{-n}$ )	$n_1$	$R_{t1}$ ( $\Omega \cdot \text{cm}^2$ )	$Q_2$ ( $\Omega^{-1} \cdot \text{cm}^{-2} \cdot \text{s}^{-n}$ )	$n_2$	$R_{t2}$ ( $\Omega \cdot \text{cm}^2$ )
0	3.778	$3.525 \times 10^{-4}$	0.8095	339.7	$4.139 \times 10^{-4}$	0.8605	$1.235 \times 10^3$
0.05	2.635	$9.385 \times 10^{-5}$	0.8912	1181	$8.11 \times 10^{-5}$	0.7919	$5.854 \times 10^4$
0.1	2.738	$9.959 \times 10^{-5}$	0.8807	795.9	$1.182 \times 10^{-4}$	0.7947	$4.083 \times 10^4$
0.5	1.655	$1.232 \times 10^{-4}$	0.8973	530.7	$1.709 \times 10^{-4}$	0.8534	$1.759 \times 10^4$

EIS is a commonly used nondestructive electrochemical detection method. In general, the low-frequency loop in the EIS plots reflects the speed control steps of the corrosion process, and the high-frequency loop represents the information of the corrosion product film [27-28]. Figure 5 shows the Nyquist plots of the base and weld metals with different  $S^{2-}$  concentrations. The corresponding Bode plots are shown in Figure 6. For all conditions, the Nyquist plot consists of two capacitor loops in the intermediate and low frequencies, which are in good agreement with the two time constants in the Bode plots of the phase angles (Figure 6). Note that some Bode plots show one wide peak, which could be considered a superposition of two peaks. The diameter of the capacitive loops decreased with increasing  $S^{2-}$  concentration, except that relatively small capacitive loops were observed on the weld metal with no  $S^{2-}$  presence.

The EIS fitting was carried out by using the equivalent circuit shown in Figure 8 [29-30], where  $R_s$  is the solution resistance,  $R_{t1}$  and  $Q_1$  are the corrosion product film resistance (low-frequency capacitive loop) and the constant phase element (CPE), respectively, and  $Q_2$  and  $R_{t2}$  are the CPE and charge transfer resistance (intermediate frequency capacitance loop), respectively. The CPE is usually used as a substitute for a capacitor to compensate for its nonideal capacitive response. The impedance of the CPE is defined as  $Z_{CPE} = [Q(j\omega)^n]^{-1}$ , where  $Q$  is the capacitance,  $\omega$  is the angular frequency ( $\text{rad s}^{-1}$ ), and  $n$  is the exponential term ( $0 < n \leq 1$ ).

According to the proposed equivalent circuit model, all the EIS curves were fitted with the values of the fitting parameters listed in Tables 2 and 3. The solution resistance ( $R_s$ ) decreased with an increasing  $S^{2-}$  concentration, indicating that the addition of  $\text{Na}_2\text{S}$  improved the conductivity of the solution. For the base metal, the  $R_{t1}$  and  $R_{t2}$  values were  $1.894 \times 10^5$  and  $1.075 \times 10^5 \Omega \cdot \text{cm}^2$ , respectively, without the addition of  $S^{2-}$ . When  $S^{2-}$  was added into the solution, the  $R_{t1}$  and  $R_{t2}$  values both decreased with

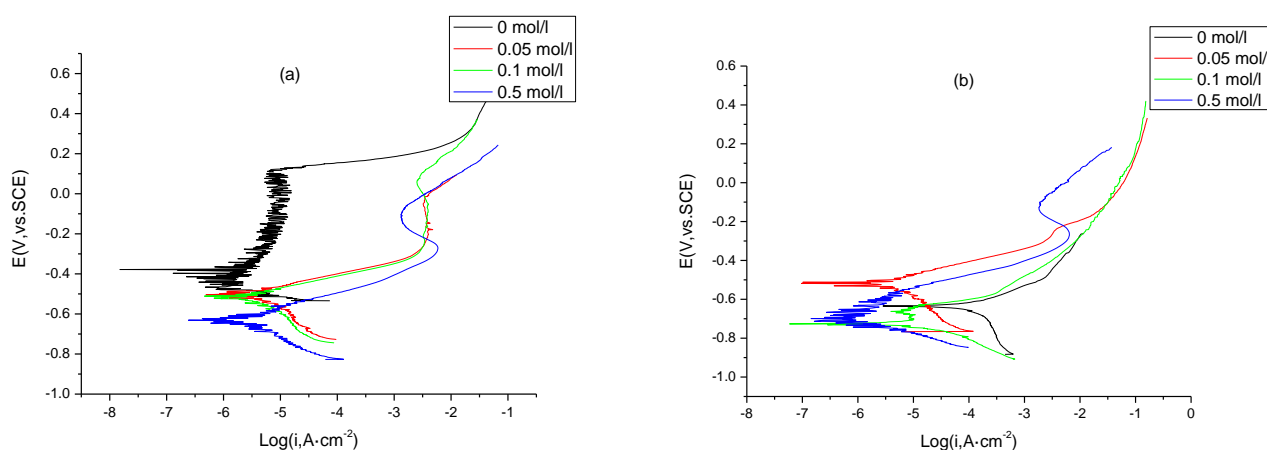
increasing  $S^{2-}$  concentration. This result confirmed that the concentration of  $S^{2-}$  had a significant influence on the corrosion resistance of the base metal. In regard to the weld metal, the  $R_{t1}$  and  $R_{t2}$  values were as low as 339.7 and  $1.235 \times 10^3 \Omega \cdot \text{cm}^2$ , respectively, without the presence of  $S^{2-}$ . The values increased to 1181 and  $5.854 \times 10^4 \Omega \cdot \text{cm}^2$  after the addition of 0.05 mol/l  $S^{2-}$ . However, the  $R_{t1}$  and  $R_{t2}$  values both decreased when the concentration of  $S^{2-}$  was further increased. These results demonstrated that a low concentration of  $S^{2-}$  could increase the corrosion resistance of the weld metal, but a high concentration of  $S^{2-}$  would decrease it, which was consistent with the trend of the polarization curves. This result might be due to the formation of a protective FeS layer when the  $S^{2-}$  concentration was low. With increasing  $S^{2-}$  concentration, the corrosion products transformed into  $\text{Fe}_{1-x}\text{S}$ , which was loose and easily fell off, leading to an increase in the corrosion rate [31].

Figure 7 shows the comparison of the Nyquist plots for the base and weld metals with different  $S^{2-}$  concentrations. The diameter of the capacitive loops for the weld metal were always smaller than that of the base metal at any given concentration. A high capacitance arc radius usually reflected a high corrosion resistance[32]. Similarly, the  $R_{t1}$  and  $R_{t2}$  values of the weld metal were both smaller than that of the base metal, as shown in Tables 2-3. This result meant that the corrosion resistance of the weld metal was lower than that of the base metal.

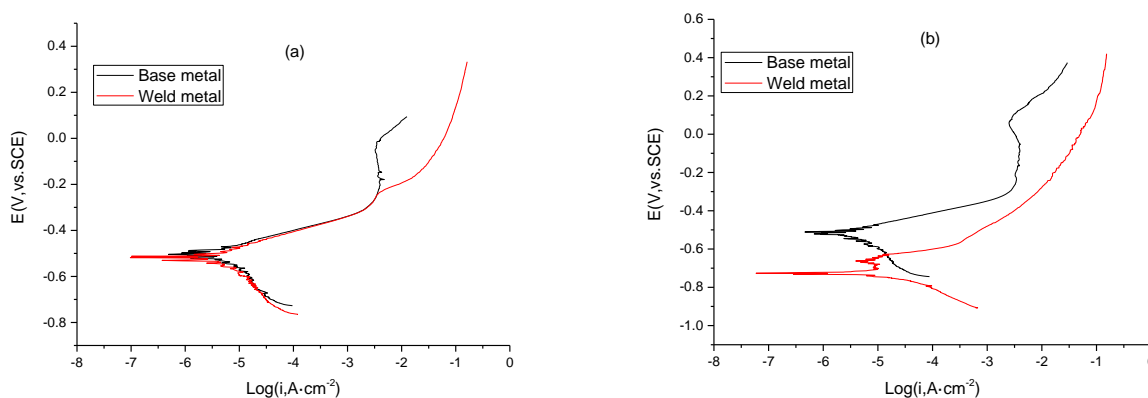
### 3.2 Influence of the $S^{2-}$ concentration on the corrosion behavior in the solution saturated with $\text{CO}_2$

Figure 9 shows the potentiodynamic polarization curves of the base and weld metals in a  $\text{CO}_2$ -saturated solution with different  $S^{2-}$  concentrations. The fitting parameters are listed in Table 4. This test demonstrated that for the base metal, the anodic branches of the polarization curves exhibited passivation to some extent, especially at a  $S^{2-}$  concentration of zero. The  $E_{\text{corr}}$  value was negatively shifted, but the  $i_{\text{corr}}$  value showed an increasing trend with an increasing  $S^{2-}$  concentration. This result meant that the electrochemical reaction rate of the base metal increased with a high concentration of  $S^{2-}$ . For the weld metal, the occurrence of slight passivation was only observed at 0.5 mol/l  $S^{2-}$ . In Figure 10, potentiodynamic polarization curves between the base and weld metals in  $\text{CO}_2$ -saturated solution with different concentrations of  $S^{2-}$  were compared. Their trends and shapes were similar, especially at concentrations of 0.05 and 0.5 mol/l. The fitting results revealed that the corrosion current density ( $i_{\text{corr}}$ ) of the weld metal was higher than that of the base metal at  $S^{2-}$  concentrations of 0, 0.05 and 0.1 mol/l. Nevertheless, the  $i_{\text{corr}}$  of the weld metal was low when the concentration was 0.5 mol/l. This result implied that the electrode reaction was suppressed when the  $S^{2-}$  concentration was high. The corrosion current density of the base and weld metals in the  $\text{CO}_2$ -free or  $\text{CO}_2$ -saturated solutions with different concentrations of  $S^{2-}$  are shown in Figure 8 to further reveal the effect of the  $\text{CO}_2$  and  $S^{2-}$  concentrations on corrosion. It was found that 1) welding increased the corrosion rate of the sample except for the weld metal in a  $\text{CO}_2$ -saturated solution with a  $S^{2-}$  concentration of 0.5 mol/l, and 2) the synergistic effect of  $\text{CO}_2$  and  $S^{2-}$  on accelerating corrosion prevailed at low  $S^{2-}$  concentrations, while a synergistic inhibition effect could occur at a high  $S^{2-}$  concentration of 0.5 mol/l [33-34]. Similar results were reported elsewhere[33-34]. It was reported that FeS and/or  $\text{FeCO}_3$  scales could form on the steel surface, depending on the concentration or pressure of  $S^{2-}$  and  $\text{CO}_2$ . When the  $S^{2-}$  concentration was low ( $< 0.1$

mol/l), the corrosion process was governed by CO<sub>2</sub> corrosion, with FeCO<sub>3</sub> being the main product along with a small amount of FeS. In this scenario, the protection from the above scales was very limited, and the corrosion current increased because of the additional corrosion caused by S<sup>2-</sup>. However, a protective FeS scale could be formed in addition to FeCO<sub>3</sub> at a S<sup>2-</sup> concentration of 0.5 mol/l, which could effectively protect the steel surface. Under the synergy between 0.5 ml/l of S<sup>2-</sup> and CO<sub>2</sub>, the corrosion rate of the weld metal significantly declined, and the base metal slightly declined compared to the sample tested with 0.5 mol/l S<sup>2-</sup> in the absence of CO<sub>2</sub> (Table 4). This result implied that the formation of FeS and FeCO<sub>3</sub> scales was more pronounced on the weld metal. Note that the polarization curve of the weld metal was not smooth but featured fluctuations with a S<sup>2-</sup> concentration of 0.5 mol/l, implying the occurrence of complex electrochemical reactions on the sample surface (Figure 9(b)).



**Figure 9.** Potentiodynamic polarization curves of the base (a) and weld metals (b) in the CO<sub>2</sub>-saturated solution with different concentrations of S<sup>2-</sup> at 60 °C



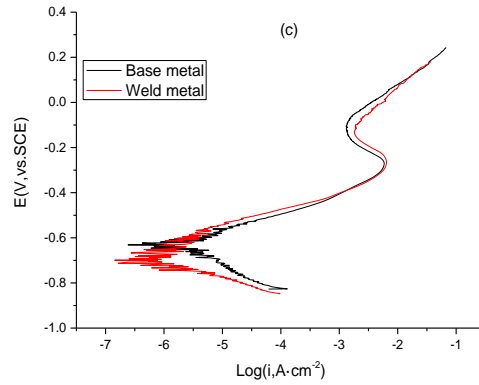


**Figure 10.** Comparison of the potentiodynamic polarization curves between the base and weld metals in the CO<sub>2</sub>-saturated solution with different concentrations of S<sup>2-</sup> at 60 °C: (a) 0.05 mol/l, (b) 0.1 mol/l, and (c) 0.5 mol/l.

**Table 4.** Fitting parameters of the potentiodynamic polarization curves for samples in the CO<sub>2</sub>-saturated solution with different S<sup>2-</sup> concentrations at 60 °C

S <sup>2-</sup> concentration (mol/l)	Material	E <sub>corr</sub> (V <sub>SCE</sub> )	i <sub>corr</sub> (μA·cm <sup>-2</sup> )	β <sub>a</sub> (mV·decade <sup>-1</sup> )	β <sub>c</sub> (mV·decade <sup>-1</sup> )
0	Base metal	-0.378	2.576	540	45
	Weld metal	-0.634	162	109	706
0.05	Base metal	-0.504	2.887	60	1310
	Weld metal	0.518	4.138	70	215
0.1	Base metal	-0.512	3.981	56	213
	Weld metal	0.726	32.35	170	130
0.5	Base metal	-0.613	4.344	80	130
	Weld metal	-0.708	0.177	60	70

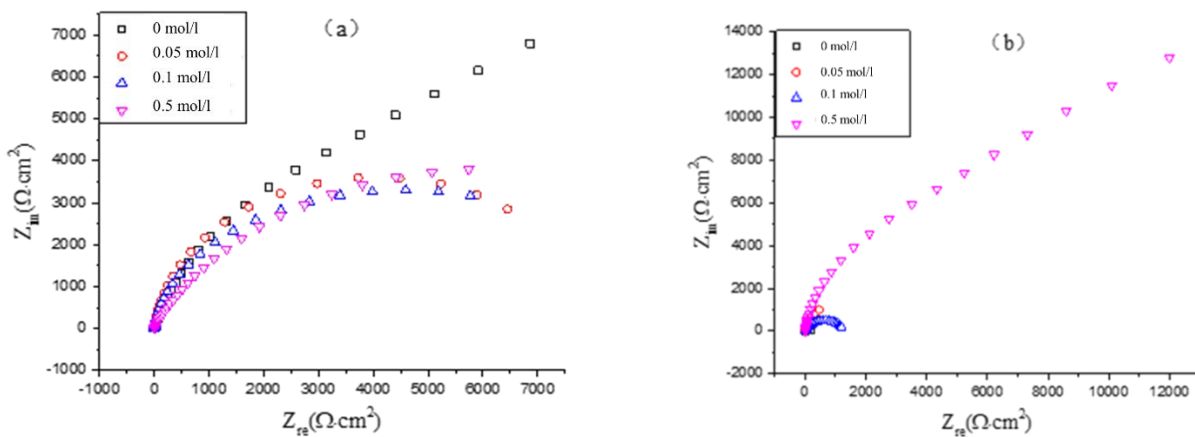


**Figure 11.** Nyquist plots of the base (a) and weld metals (b) in the CO<sub>2</sub>-saturated solution with different S<sup>2-</sup> concentrations at 60 °C

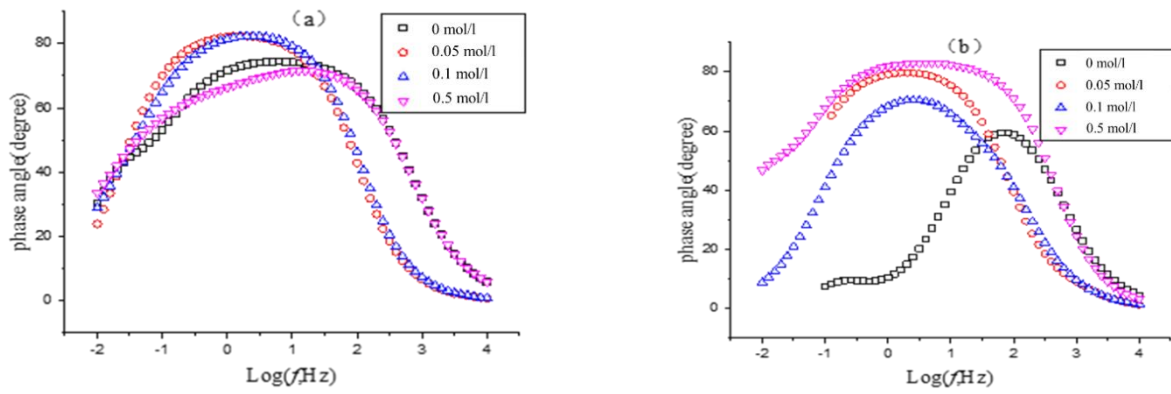


**Figure 12.** Bode plots of the base (a) and weld metals (b) in the CO<sub>2</sub>-saturated solution with different S<sup>2-</sup> concentrations at 60 °C

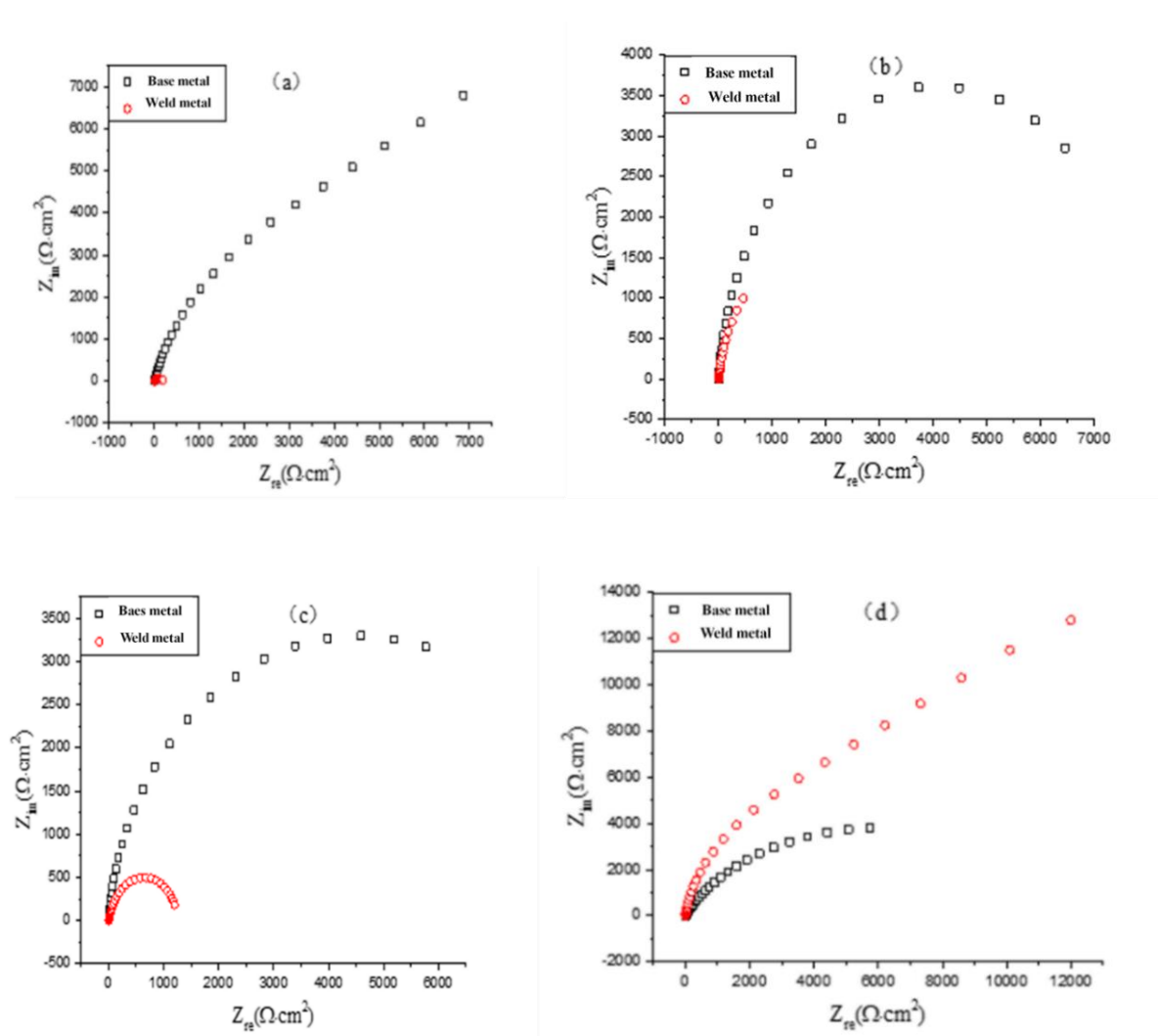


**Figure 13.** Comparison of the Nyquist plots for the base and weld metals in the CO<sub>2</sub>-saturated solution with different S<sup>2-</sup> concentrations at 60 °C: (a) 0 mol/L, (b) 0.05 mol/L, (c) 0.1 mol/L, and (d) 0.5 mol/L

Figures 11 and 12 display the Nyquist and Bode plots of the base and weld metals in the CO<sub>2</sub>-saturated solution with different S<sup>2-</sup> concentrations. Similar to the samples tested in the CO<sub>2</sub>-free solution, two overlapping capacitive loops in the medium and low-frequency ranges could be identified, although some Bode plots showed a wide peak that was a superposition of two peaks. The EIS data were fitted with the same electrochemical equivalent circuit model as that in the CO<sub>2</sub>-free solution (Figure 8), where R<sub>s</sub> represents the solution resistance, R<sub>t1</sub> and Q<sub>1</sub> are the corrosion product film resistance (low-frequency capacitive loop) and the constant phase element (CPE), respectively, and Q<sub>2</sub> and R<sub>t2</sub> are the CPE and charge transfer resistance (medium-frequency capacitive loop), respectively. The fitted parameters are listed in Tables 5 and 6.

**Table 5.** EIS parameters of the base metal in the CO<sub>2</sub>-saturated solution with different S<sup>2-</sup> concentrations at 60 °C

S <sup>2-</sup> concentration (mol/l)	R <sub>s</sub> (Ω·cm <sup>2</sup> )	Q <sub>1</sub> (Ω <sup>-1</sup> ·cm <sup>-2</sup> ·s <sup>-n</sup> )	n <sub>1</sub>	R <sub>t1</sub> (Ω·cm <sup>2</sup> )	Q <sub>2</sub> (Ω <sup>-1</sup> ·cm <sup>-2</sup> ·s <sup>-n</sup> )	n <sub>2</sub>	R <sub>t2</sub> (Ω·cm <sup>2</sup> )
0	3.694	2.118×10 <sup>-4</sup>	0.8494	1.164×10 <sup>4</sup>	7.326×10 <sup>-4</sup>	1	1.122×10 <sup>4</sup>
0.05	3.045	7.502×10 <sup>-4</sup>	0.9403	7761	0.01776	1	1.370×10 <sup>4</sup>
0.1	2.896	6.685×10 <sup>-4</sup>	0.9473	4335	7.869×10 <sup>-4</sup>	0.6004	1.567×10 <sup>4</sup>
0.5	1.788	4.502×10 <sup>-4</sup>	0.8461	789.3	2.888×10 <sup>-4</sup>	0.5822	1.18×10 <sup>4</sup>

**Table 6.** EIS parameters of the weld metal in the CO<sub>2</sub>-saturated solution with different S<sup>2-</sup> concentrations at 60 °C

S <sup>2-</sup> concentration (mol/l)	R <sub>s</sub> (Ω·cm <sup>2</sup> )	Q <sub>1</sub> (Ω <sup>-1</sup> ·cm <sup>-2</sup> ·s <sup>-n</sup> )	n <sub>1</sub>	R <sub>t1</sub> (Ω·cm <sup>2</sup> )	Q <sub>2</sub> (Ω <sup>-1</sup> ·cm <sup>-2</sup> ·s <sup>-n</sup> )	n <sub>2</sub>	R <sub>t2</sub> (Ω·cm <sup>2</sup> )
0	4.71	1.935×10 <sup>-5</sup>	0.861	161.6	2.03×10 <sup>-4</sup>	0.9979	4.83×10 <sup>2</sup>
0.05	2.555	2.721×10 <sup>-4</sup>	1	101.7	7.701×10 <sup>-4</sup>	0.8855	3.736×10 <sup>2</sup>
0.1	2.926	1.246×10 <sup>-4</sup>	0.8346	87.33	1.02×10 <sup>-4</sup>	1	1.193×10 <sup>2</sup>
0.5	1.782	3.255×10 <sup>-4</sup>	0.9361	1.404×10 <sup>4</sup>	7.37×10 <sup>-4</sup>	0.9129	2.611×10 <sup>4</sup>

For the base metal in the presence of CO<sub>2</sub>, the R<sub>t1</sub> and R<sub>t2</sub> values were 1.164×10<sup>4</sup> and 1.122×10<sup>4</sup> Ω·cm<sup>2</sup>, respectively, with a S<sup>2-</sup> concentration of 0 mol/l. When the S<sup>2-</sup> concentration increased, the R<sub>t1</sub> values decreased remarkably, while the R<sub>t2</sub> values decreased slightly. For the weld metal in the presence of CO<sub>2</sub>, both the R<sub>t1</sub> and R<sub>t2</sub> values decreased with increasing S<sup>2-</sup> concentration (< 0.1 mol/l). When a high S<sup>2-</sup> concentration of 0.5 mol/l was achieved, the R<sub>t1</sub> and R<sub>t2</sub> values increased sharply to 1.404×10<sup>4</sup> and 2.611×10<sup>4</sup> Ω·cm<sup>2</sup>, indicating a high resistance to corrosive attack. This result could be due to the accumulation of S<sup>2-</sup>, which led to the formation of a new FeS film, and the formation rate of iron sulfide increased [35]. Under these circumstances, the presence of CO<sub>2</sub> and S<sup>2-</sup> might exert a synergistically beneficial effect on inhibiting the corrosion of the weld metal because the FeS film demonstrated a good

protective effect on the metal matrix.

Figure 13 shows the comparison of the Nyquist plots for the base and weld metals in the CO<sub>2</sub>-saturated solution with different S<sup>2-</sup> concentrations. The diameters of the capacitive loops for the weld metal were smaller than that of the base metal when the S<sup>2-</sup> concentration was lower than 0.1 mol/l, indicating the poor corrosion resistance of the weld metal. When the concentration of S<sup>2-</sup> was 0.5 mol/l, the diameters of the capacitive loops for the weld metal were larger than that of the base metal, indicating that the corrosion resistance of the weld metal was higher than that of the base metal. The possible reasons for this abnormal phenomenon are as follows. A passivation film was formed rapidly on the surface when the metal was immersed in the corrosive solution [36]. The protective property of the passive film on the weld metal was better than that on the base metal at a S<sup>2-</sup> concentration of 0.5 mol/l, making the corrosion resistance of the weld metal better than that of the base metal. Based on the above analysis, it was believed that the synergistic acceleration effect of CO<sub>2</sub> and S<sup>2-</sup> on metal corrosion was prominent at S<sup>2-</sup> concentrations lower than 0.1 mol/l, whereas the synergistic inhibition of corrosion could occur, especially on the weld metal, at S<sup>2-</sup> concentrations higher than 0.5 mol/l.

#### 4. CONCLUSIONS

(1) The potential polarization curve shows that the ( $E_{\text{corr}}$ ) corrosion potential of the weld metal is more negative and the corrosion current density ( $i_{\text{corr}}$ ) is higher than that of the base metal, thereby indicating a higher corrosion rate of the weld metal. Electrochemical impedance spectroscopy (EIS) shows that the charge transfer resistance of the base metal is higher than that of the weld metal; thus, the electrochemical reaction rate is smaller than that of the weld metal.

(2) With increasing S<sup>2-</sup> concentration, the corrosion potential ( $E_{\text{corr}}$ ) of the base metal negatively shifts. Moreover, the corrosion current density ( $i_{\text{corr}}$ ) increases, while the charge transfer resistance decreases, thereby exhibiting a faster corrosion rate. For the weld metal, the corrosion rate decreases with the addition of S<sup>2-</sup>. However, the corrosion current density ( $i_{\text{corr}}$ ) shows an increasing trend with an increasing S<sup>2-</sup> concentration. When the S<sup>2-</sup> concentration is increased to 0.5 mol/l, the corrosion rate decreases again.

(3) It is observed that the synergistic acceleration effect of CO<sub>2</sub> and S<sup>2-</sup> on metal corrosion is prominent at S<sup>2-</sup> concentrations lower than 0.1 mol/l, whereas the synergistic inhibition effect on corrosion can occur, especially on the weld metal, at S<sup>2-</sup> concentrations higher than 0.5 mol/l.

#### ACKNOWLEDGEMENTS

This work was jointly sponsored by Guangxi Key Laboratory of Information Materials (Guilin University of Electronic Technology), P.R. China (Project No. 191009-K), and Scientific Research Foundation and Opening Foundation (X151519KCL23) of Southwest Petroleum University.

#### References

1. X.Y. Cao, J. Deng and C.H. Shang guan, T.L. Li and L. Cui, *Steel Pipe*, 43 (2014) 11.

2. J.D. Majumdar, and L. Li, *Metallurgical and Materials Transactions A*, 40 (2009) 3001.
3. J.D. Majumdar, A. Pinkerton, Z. Liu, I. Manna and L. Li, *Applied Surface Science*, 247 (2005) 320.
4. J.W. Tang, Y.W. Shao, T. Zhang, G.Z. Meng and F.H. Wang, *Journal of Chinese Society for Corrosion and Protection*, 30 (2010) 246.
5. E. Mohammadi-Zahrani, A. Saatchi and A. Alfantazi, *Engineering Failure Analysis*, 17 (2010) 810.
6. Z. Liu, X. Gao, L. Du, J. Li, P. Li, C. Yu, R.D.K. Misra and Y. Wang, *Electrochimica Acta*, 232 (2017) 528.
7. S.L. Wang, F. Wang, F. Xu, M.Y. Bao, L. Liu, X. Wang and C.Q. Ren, *International Journal of Electrochemical Science*, 12 (2017) 10084.
8. Y.C. Liu, B. Zhang, Y.L. Zhang, L.L. Ma and P.Y. ang, *Engineering Failure Analysis*, 60 (2016) 307.
9. Y.S. Choi, S. Hassani, T.H. Vu, S. Nestic and A.Z.B. Abas, *Corrosion*, 72 (2016) 999.
10. G.A. Zhang, D. Li, Y.Z. Li and X.P. Guo, *Corrosion Science*, 120 (2017) 107.
11. S.L. Wang, L. Wang, X.G. Liu, M.Y. Bao, L. Liu, X. Wang and C.Q. Ren, *International Journal of Electrochemical Science*, 12 (2017) 10317.
12. M. Liu, J.Q. Wang, W. Ke and E.H. Han, *Journal of Materials Science & Technology*, 30 (2013) 504.
13. S.M. Abd-El-Haleem and E.E. Abd-El-Aal, *Corrosion Engineering Science and Technology*, 43 (2008) 173.
14. A. Davoodi, M. Pakshir, M. Babaiee and G.R. Ebrahimi, *Corrosion Science*, 53 (2011) 399.
15. W. Liu, X.L. Pu, X.D. Bai and H.W. Zhang, *Petroleum Drilling Techniques*, 36 (2008) 83.
16. L. Liu, M.Y. Wang, Z. Wang and Y. Zhang, *Hydrometallurgy*, 157 (2015) 285.
17. E. Abelev, J. Sellberg, T.A. Ramanarayanan, T.A. Ramanarayanan and S.L. Bernasek, *Journal of Materials Science*, 44 (2009) 6167.
18. X.S. Huang, Y.M. Qi, C.F. Chen, H.B. Yu and G.W. Lu, *Corrosion Engineering Science and Technology*, 50(2015) 169.
19. Q.F. Wang, Z. Pu, M.B. Shuai and D.M. Lang, *Rare Metal Materials and Engineering*, 43(2014)393.
20. L. Wu, F.Q. Xie, X.F. Yao and X.Q. Wu, *Materials Reports*, 12 (2013) 121.
21. D.J. Wu, C. Fan, S.B. Liu, G.Y. Ma and D.M. Guo, *The Chinese Journal of Nonferrous Metals*, 24 (2014) 441.
22. C.P. Liu and X. Han, *Industrial Water Treatment*, 39 (2019) 57.
23. A.F. Ballesteros, J.A.P. Gomes and I.S. Bott, *Materials Research-ibero-american Journal of Materials*, 18 (2015) 417.
24. N.M. Lin, L.L. Zhao, Q. Liu, J.J. Zou, R.Z. Xie, S. Yuan, D. Li, L.X. Zhang, Z.H. Wang and B. Tang, *Journal of Physics & Chemistry of Solids*, 129(2019)387.
25. R. Wang, S.J. Luo, M. Liu and Y. Xue, *Corrosion Science*, 85(2014)270.
26. Y.H. Kim, D.G. Kim, J.H. Sung, I.S. Kim, D.E. Ko, N.H. Kong, H.U. Hong, J.H. Park and H.W. Lee, *Metals and Materials International*, 17 (2011) 151.
27. M.C. Yan, C. Sun, J.H. Dong, J. Xu, W. Ke, *Corrosion Science*, 97(2015)62.
28. S. Wang, X. Yin, H. Zhang, D. Liu, N. Du, *Materials (Basel, Switzerland)*, 12(2019)1996.
29. W. Zhao, Y. Zou, K. Matsuda and Z.D. Zou, *Materials & Design*, 99 (2016) 44.
30. J.B. Wang, G.C. Xiao, W. Zhao, B.R. Zhang and W.F. Rao, *Metals*, 9 (2019) 1325.
31. X.D. Zhao, K.F. Chen, J. Yang, G.F. Xi, J. Sun and H.T. Tian, *RSC Advances*, 8(2018)38118.
32. Y. Wang, M.Y. Li, F. Zhu, W.T. Dong, X.Y. Zhang and L.L. Sun, *Surface & Coatings Technology*, 385(2020)0257.
33. Y.S. Choi, S. Nestic and S. Ling, *Electrochimica Acta*, 56 (2017) 1752.
34. W.F. Li, Y.J. Zhou and Y. Xue, *Journal of Iron and Steel Research International*, 19 (2012) 59.
35. Z.G. Liu, X.H. Gao, L.X. Du, J.P. Li, P. Li, C. Yu, R.D.K. Misra and Y.X. Wang, *Electrochimica Acta*, 232(2017)528.

36. A. Fattah-Alhosseini, A. Saatchi, M.A. Golozar and K. Raeissi, *Journal of Applied Electrochemistry*, 40 (2010) 457.

© 2020 The Authors. Published by ESG ([www.electrochemsci.org](http://www.electrochemsci.org)). This article is an open access article distributed under the terms and conditions of the Creative Commons Attribution license (<http://creativecommons.org/licenses/by/4.0/>).